Engineering Fracture Mechanics 284 (2023) 109202

Contents lists available at ScienceDirect

Engineering Fracture Mechanics

journal homepage: www.elsevier.com/locate/engfracmech

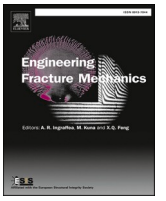

Gypsum and quartz specimens in compression failure: Fracto-emissions and related stoichiometric balances

Alberto CARPINTERI [a,b,*], Oscar BORLA [c], Federico ACCORNERO [d]

[a] Chair Professor, DISEG, Politecnico di Torino, Turin, Italy
[b] Zhujiang (Pearl River) Professor of Guangdong Province, Dept of Civil and Environmental Engineering, Shantou University, Shantou, P.R. China
[c] Graduate Technician, DISEG Service Centre, Politecnico di Torino, Turin, Italy
[d] Associate Professor, College of Engineering, Shantou University, Shantou, P.R. China

ARTICLE INFO

Keywords:
Brittle failure
Fracto-emissions
LENR

ABSTRACT

Extensive experimental investigations were conducted on Gypsum and Quartz compression specimens of different sizes. They were brought to complete failure, showing two different failure modalities: (1) Very brittle loading drop for micro-crystalline Gypsum and Quartz; (2) Stable strain-softening behaviour for macro-crystalline Gypsum. All the tested specimens emitted acoustic and electromagnetic waves and the single events cumulated up to the peak load. On the other hand, neutron emissions were evident only for the largest specimens. The significant chemical composition changes occurring on the fracture surfaces are consistently explained by the assumption of Low-energy Nuclear Reactions (LENR), both fusion and fission. It is the first time that fusion reactions emerge from crushing tests, whereas fission reactions have already consistently explained the results related to other materials like the iron-rich natural rocks. Therefore, a correlation emerges between fusion nuclear reactions and strain-softening mechanical behaviour, as well as between fission nuclear reactions and brittle mechanical behaviour.

1. Introduction

It is possible to demonstrate experimentally that the failure phenomena, in particular when they occur in a brittle way, i.e. with a mechanical energy emission, emit additional forms of energy related to the fundamental natural forces. The authors have found experimental evidence and confirmation that energy emission of different forms occurs from solid-state fracture. The tests were carried out at the Laboratory of Fracture Mechanics of the Politecnico di Torino, Italy. By subjecting quasi-brittle materials such as Gypsum and Quartz to compression tests, bursts of neutron emission (NE) during the failure process were observed [1–5], necessarily involving nuclear reactions, besides the well-known acoustic emission (AE) [6–13], and the phenomenon of electromagnetic radiation (EME) [14–19], which is highly suggestive of charge redistribution during material failure. The phenomenon of EME is regarded as an

Abbreviations: AE, Acoustic Emissions; C, Carbon; Ca, Calcium; cps, counts per second; EDS, Energy Dispersive X-ray Spectroscopy; EDX, Energy-dispersive X-ray Detector; EME, Electromagnetic Emissions; FESEM, Field Emission Scanning Electron Microscope; Hz, Hertz; kHz, kiloHertz; LENR, Low-energy Nuclear Reactions; Mg, Magnesium; MHz, MegaHertz; N, Nitrogen; NE, Neutron Emissions; NIM, Nuclear Instrument Module; O, Oxygen; S, Sulfur; Si, Silicon; THz, TeraHertz; TTL, Transistor-transistor Logic; PZT, Piezoelectric Transducer.

* Corresponding author.
E-mail address: alberto.carpinteri@polito.it (A. CARPINTERI).

https://doi.org/10.1016/j.engfracmech.2023.109202
Received 14 October 2022; Received in revised form 9 March 2023; Accepted 14 March 2023
Available online 20 March 2023

Fig. 1. Gypsum specimens varying the slenderness (left) and Quartz specimens with irregular shapes (right).

Table 1
Tested specimens and their geometrical and mechanical characteristics.

Specimen Type	Number of Specimens	Dimensions		Piston Velocity	Volume	Average Peak Load
		Diameter [mm]	Slenderness λ	[m/s]	[mm^3]	[kN]
Gypsum (micro-crystalline)						
G-50–0.5-micro	3	50	0.5	1×10^{-6}	49,062	72.52 ± 3.65
G-50–1.0-micro	3	50	1.0	1×10^{-6}	98,125	55.35 ± 2.20
G-50–2.0-micro	3	50	2.0	1×10^{-6}	196,250	44.80 ± 3.83
Gypsum (macro-crystalline)						
G-50–1.0-macro	3	50	1.0	1×10^{-6}	98,125	52.19 ± 4.47
G-50–2.0-macro	3	50	2.0	1×10^{-6}	196,250	49.03 ± 3.61
Quartz						
Q-40–1.5	5	40	1.5	1×10^{-6}	75,360	168.07 ± 18.74

important precursor of critical phenomena in Geophysics, such as rock fractures, volcanic eruptions, and earthquakes [19,20]. For example, anomalous radiations of geo-electromagnetic waves were observed before major earthquakes. At the laboratory scale, rocks and concrete under compression generate AE and EME nearly simultaneously. This evidence suggests that also NE are generated during crack growth, reinforcing the idea that the NE phenomenon can be applied as a forecasting tool for earthquakes.

While the mechanism of AE is fully understood, being provided by transient elastic waves due to stress redistribution following fracture propagation [6–13], the origin of EME from fracture is not completely clear and different attempts have been made to explain it.

An explanation of the EME origin was related to dislocation phenomena [16], which however are not able to explain EME from fracture in brittle materials, where the motion of dislocations is negligible [17]. Frid et al. [17] and Rabinovitch et al. [21] recently proposed a model of the EME origin where, following the rupture of bonds during the crack growth, mechanical and electrical equilibrium are broken at the fracture surfaces with the creation of ions moving collectively as a surface wave on both faces. The resulting oscillating dipoles created on both faces of the propagating fracture act as the source of EME.

As regards the neutron emissions, in this paper we present experimental tests performed on brittle rocks (Gypsum and Quartz), using a He3 neutron device and a bubble type BD thermodynamic neutron detector. For brittle specimens of sufficiently large dimensions and/or slenderness, neutron emissions, detected by He3, were found to be up to three/four times higher than the natural background at the time of the failure. These emissions fully confirm the previous tests [1–5] and are due to Low-energy Nuclear Reactions (LENR), which depend on the different modalities of mechanical energy release during the tests. For specimens with sufficiently large size and slenderness, a relatively high mechanical energy emission is expected, and hence a higher probability of neutron emissions at the time of failure. The formation of coherent EME fields occurs over a wide range of frequencies, from few Hz to MHz, and even up to microwave frequencies. This excited state of the matter could be one of the causes of subsequent resonance phenomena of the nuclei able to produce neutron bursts. This hypothesis was also confirmed by Widom et al. [22,23]. As a matter of fact, the microcracking elastic energy emission and the related acoustic vibrations are converted into electromagnetic oscillations. The electromagnetic waves, generated during microcracking, accelerate the condensed matter electrons, which then collide with protons producing neutrons and neutrinos [22,23]. Carpinteri and Lucia [24,25] recently considered a model where THz frequencies are reached by phonons as well as by plasmons with the possibility of coupling interactions with atomic lattices and nuclei. Carpinteri and Borla [26–28] explained through LENR the geochemical evolution of our planet, which is due to the most critical tectonic events. As in Geochemistry so in Electrochemistry, nano- and microcracking of the electrodes produce THz vibrations and LENRs with sub-atomic particle emissions [29].

Table 2
Tested specimens and their fracto-emission average characteristics.

Specimens Type	AE		EME		NE	
	Average Frequency [kHz]	Average Highest Frequency [kHz]	Average Frequency [MHz]	Average Highest Frequency [MHz]	Average Neutron Background [10^{-2} cps]	Average Count Rate at the Neutron Emission Peak [10^{-2} cps]
Gypsum (micro-crystalline)						
G-50–0.5-micro	31.84 ± 6.35	65.46 ± 7.59	37.59 ± 6.84	72.01 ± 15.25	5.20 ± 1.30	Background
G-50–1.0-micro	38.61 ± 7.64	63.01 ± 4.27	29.64 ± 10.91	76.49 ± 15.47	5.20 ± 1.30	Background
G-50–2.0-micro	35.92 ± 6.75	62.79 ± 5.85	38.66 ± 9.07	71.25 ± 12.64	5.20 ± 1.30	15.85 ± 3.96
Gypsum (macro-crystalline)						
G-50–1.0-macro	33.79 ± 6.89	79.27 ± 6.42	40.24 ± 8.46	75.69 ± 13.55	5.41 ± 1.35	Background
G-50–2.0-macro	30.96 ± 5.76	81.58 ± 7.14	38.99 ± 9.33	74.98 ± 14.99	5.41 ± 1.35	18.75 ± 4.69
Quartz						
Q-40–1.5	36.63 ± 7.72	76.22 ± 8.09	44.05 ± 10.96	77.62 ± 11.04	5.13 ± 1.28	21.11 ± 5.27

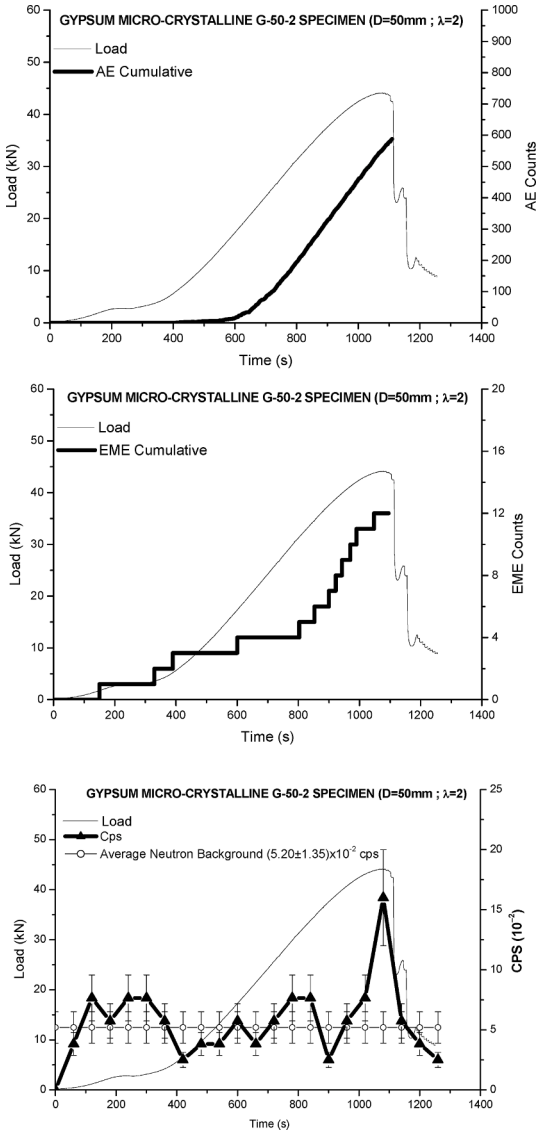

Fig. 2. Load vs time diagram of the Gypsum micro-crystalline specimen (G-50–2.0): Cumulated number of AEs (up); Cumulated number of EMEs (middle); NE count rate (down).

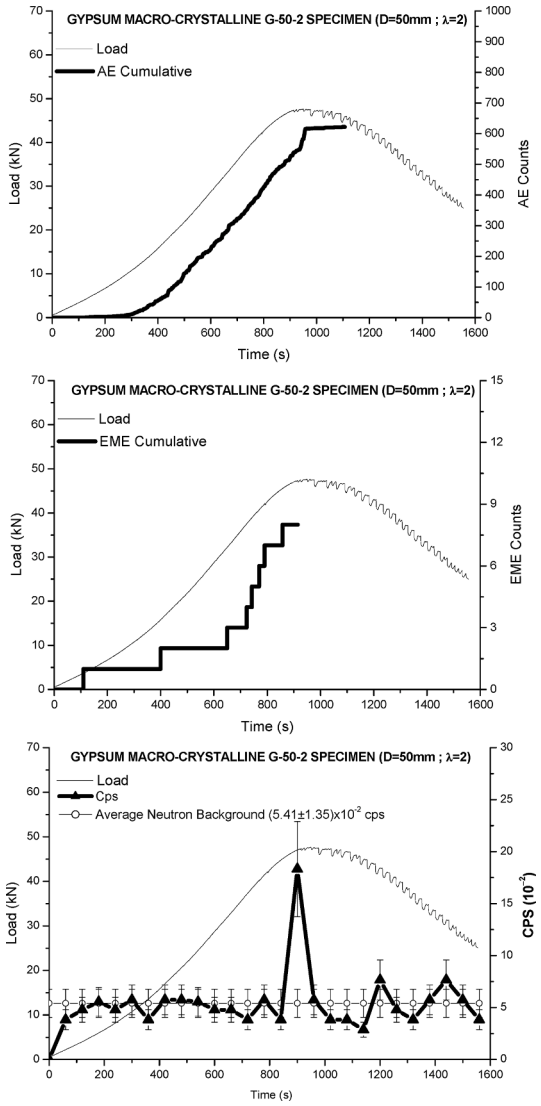

Fig. 3. Load vs time diagram of the Gypsum macro-crystalline specimen (G-50–2.0): Cumulated number of AEs (up); Cumulated number of EMEs (middle); NE count rate (down).

2. Experimental set up

Compression tests were performed on rock specimens (nine of micro-crystalline Gypsum, six of macro-crystalline Gypsum, and five of Quartz) under monotonic displacement control. The materials used for the tests are non-radioactive Gypsum (in the micro- and macro-crystalline form) and Quartz. In these tests, a total of 20 specimens with different size and slenderness are used (Fig. 1). In Tables 1 and 2, the experimental data concerning the tested specimens are summarized.

All the specimens were subjected to uniaxial compression using a servo-controlled hydraulic testing machine with a maximum capacity of 600 kN. Each test was performed in piston travel displacement control by setting a constant piston velocity. The specimens were arranged in contact with the press platens without any coupling material, according to the testing modalities known as "test by means of rigid platens with friction".

The AE activity emerging from the compressed specimens was detected by attaching to the specimen surface a piezoelectric transducer (PZT), which is able to convert the high-frequency surface vibrations due to the acoustic waves into an electric signal (the AE signal). The sensitivity of the transducer in the low-frequency range was measured by placing it on a shaker excited with all frequencies in the range 0–10 kHz (*white noise*). The result of this calibration at low frequencies was 1.2 μV/(mms^{-2}). Resonant sensors are more sensitive than broadband sensors, which are characterized by a flat frequency response in their working range, and then they can be successfully used in monitoring large-sized structures.

The EME equipment consists of a telescopic antenna, having a maximum length of 125 cm. A telescopic antenna can be considered

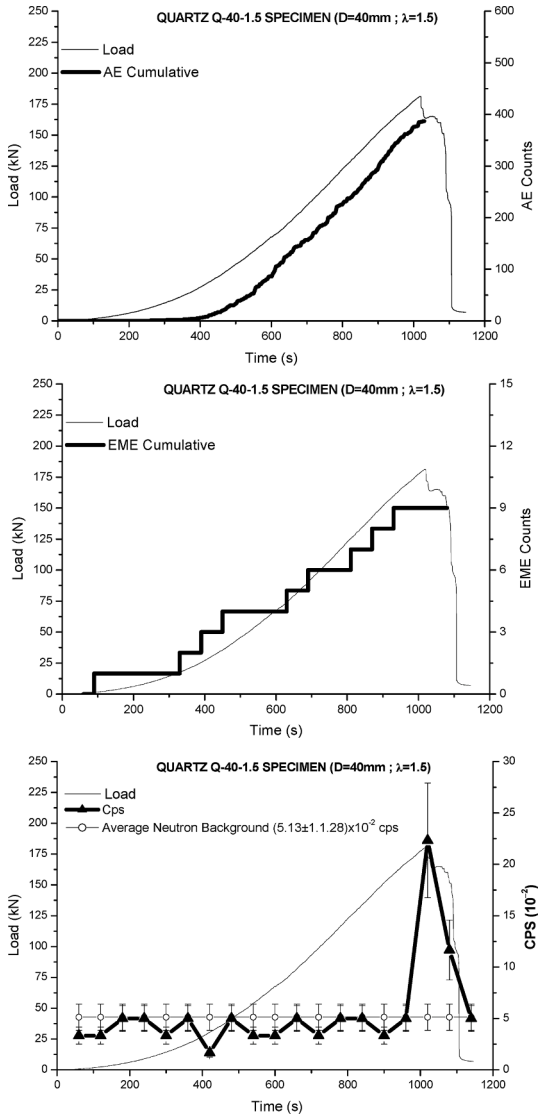

Fig. 4. Load vs time diagram of the Quartz specimen (Q-50–1.5): Cumulated number of AEs (up); Cumulated number of EMEs (middle); NE count rate (down).

as a sort of length-adjustable monopole. By pulling it to the right length, the antenna can be tuned to operate at different frequencies. For this reason, it represents a "wide band" device, in the sense that it is possible to adjust its length according to the frequency/wavelength that the operator wants to receive. Telescopic antennas are generally used for frequencies $\leq$ 500 MHz. Moreover, the antenna is coupled with an Agilent DSO1052B oscilloscope (50 MHz, 2 channels) that allows appropriate monitoring of EME signals with frequencies up to tens of MHz.

The neutron emission (NE) detector used in the compression tests under monotonic displacement control is of the He^3 type with electronics of pre-amplification, amplification, and discrimination directly connected to the detector tube. The detector is powered with 1.3 kV, supplied via a high-voltage NIM (Nuclear Instrument Module). The logic output producing the TTL (transistor-transistor logic) pulses is connected to a NIM counter. The device was calibrated for the measurement of thermal neutrons. Its sensitivity is 65 $cps/n_{thermal}$ ($\pm$10 % declared by the factory), i.e., a thermal neutron flux of 1 thermal neutron/cm^2 s corresponds to a count rate of 65 cps.

Furthermore, Energy-dispersive X-ray Spectroscopy (EDS) was carried out in order to identify possible evidence of phono-fission reactions that can take place during the compression failure. The elemental analyses were performed by a ZEISS Auriga field emission scanning electron microscope (FESEM) equipped with an Oxford INCA Energy-dispersive X-ray Detector (EDX), with a resolution of 124 eV @ MnKa. The energy used for the analyses was equal to 18 keV.

Table 3
Test performed on a micro-crystalline gypsum specimen. Element concentrations on external and fracture surfaces; Nuclear and stoichiometric balances.

Element	External surface mean value	Fracture surface mean value	Increase or decrease
	[wt%]	[wt%]	[wt%]
C	14.7	20.6	+5.9
O	60.2	55.4	–4.8
Si	1.5	0.2	–1.3
Mg	1.3	0.5	–0.8
Ca	11.2	11.2	0.0
S	11.7	11.9	+0.2

Nuclear balances

$O_8^{16} \rightarrow C_6^{12} + He_2^4$
$Si_{14}^{28} \rightarrow 2C_6^{12} + He_2^4$
$Mg_{12}^{24} \rightarrow 2C_6^{12}$

Stoichiometric balances

O (–4.8%) = C (+3.6%) + He (+1.2%)
Si (–1.3%) = C (+1.1%) + He (+0.2%)
Mg (–0.8%) = C (+0.8%)

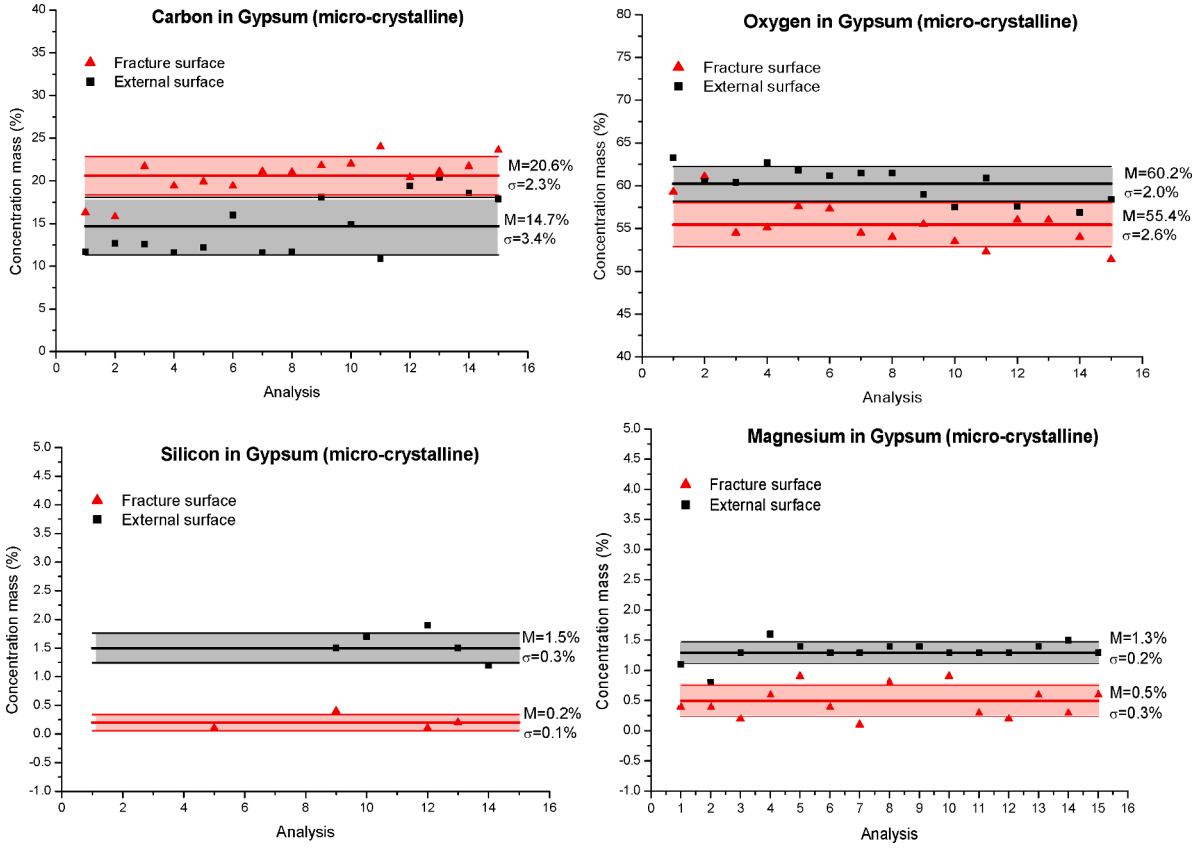

Fig. 5. EDS results for C, O, Si, and Mg concentrations in micro-crystalline gypsum: (a) C concentration on external surfaces (black squares) and on fracture surfaces (red triangles); (b) O concentration on external surfaces (black squares) and on fracture surfaces (red triangles); (c) Si concentration on external surfaces (black squares) and on fracture surfaces (red triangles); (d) Mg concentration on external surfaces (black squares) and on fracture surfaces (red triangles).

3. Test results

The tested specimens (Fig. 1) with their geometrical and mechanical characteristics are described in Table 1. The experimental diagrams reported in the following and describing load and fracto-emission measurement versus time are related to three of the total

Table 4
Test performed on a macro-crystalline gypsum specimen. Element concentrations on external and fracture surfaces; Nuclear and stoichiometric balances.

Element	External surface mean value	Fracture surface mean value	Increase or decrease
	[wt%]	[wt%]	[wt%]
C	32.7	16.1	–16.6
O	47.8	56.1	+8.3
N	1.0	0.8	–0.2
Si	0.7	0.9	+0.2
S	8.7	13.0	+4.3
Mg	0.8	1.0	+0.2
Ca	8.3	12.1	+3.8

Nuclear balances

$4C_6^{12} \rightarrow Ca_{20}^{40} + 2He_2^4$
$Ca_{20}^{40} \rightarrow S_{16}^{32} + 2He_2^4$
$S_{16}^{32} \rightarrow 2O_8^{16}$

Stoichiometric balances

C (–16.6%) = Ca (+13.8%) + He (+2.8%)
Ca (–10.0%) = S (+8.0%) + He (+2.0%)
S (–3.7%) = O (+3.7%)

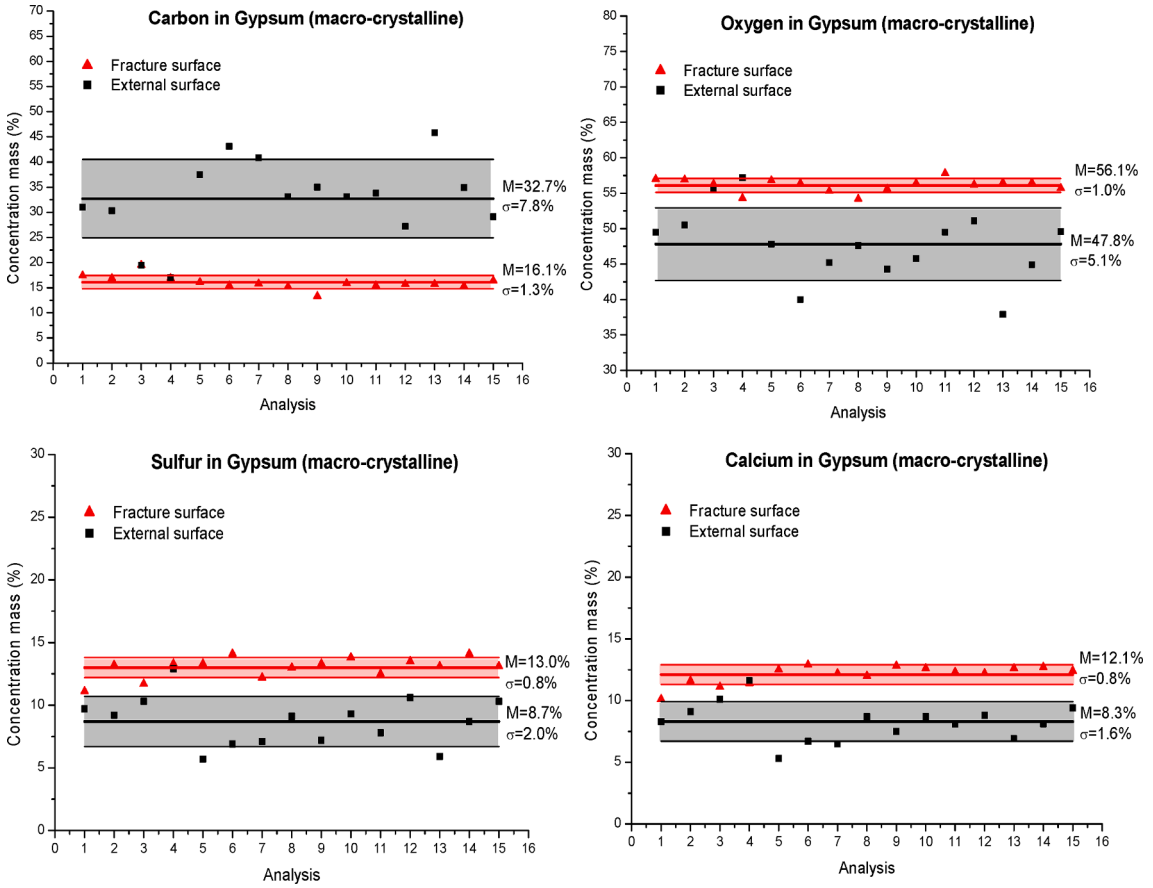

Fig. 6. EDS results for C, O, S and Ca concentrations in macro-crystalline gypsum: (a) C concentration on external surfaces (black squares) and on fracture surfaces (red triangles); (b) O concentration on external surfaces (black squares) and on fracture surfaces (red triangles); (c) S concentration on external surfaces (black squares) and on fracture surfaces (red triangles); (d) Ca concentration on external surfaces (black squares) and on fracture surfaces (red triangles).

Table 5
Test performed on a quartz specimen. Element concentrations on external and fracture surfaces; Nuclear and stoichiometric balances.

Element	External surface mean value	Fracture surface mean value	Increase or decrease
	[wt%]	[wt%]	[wt%]
C	55.6	62.1	+6.5
O	31.0	24.1	–6.9
Si	9.6	10.9	+1.3
N	1.3	0.1	–1.2
Mg	0.1	0.1	0.0
Na	0.5	0.4	–0.1
S	1.2	0.4	–0.8
Ca	0.5	0.1	–0.4

Nuclear balances

$O_8^{16} \rightarrow C_6^{12} + He_2^4$
$S_{16}^{32} \rightarrow 2C_6^{12} + 2He_2^4$
$Ca_{20}^{40} \rightarrow 3C_6^{12} + He_2^4$
$2N_7^{14} \rightarrow Si_{14}^{28}$

Stoichiometric balances

O (–6.9%) = C (+5.2%) + He (+1.7%)
S (–0.8%) = C (+0.6%) + He (+0.2%)
Ca (–0.4%) = C (+0.4%) + He (+0.0%)
N (–1.2%) = Si (+1.2%)

20 specimens (one for each material: micro-crystalline Gypsum, macro-crystalline Gypsum, and Quartz). All specimens were tested in compression up to complete failure, showing a catastrophic drop (*snap-back*) in the load carrying capacity, when deformed beyond the peak load (Figs. 2 and 4), or a softening behaviour (Fig. 3). The post-peak branch of micro-crystalline Gypsum and Quartz mechanical responses is characterized by a sharp strain localization. Experimental evidence emerges of AE, EME, and NE activities. In Figs. 2, 3, and 4, AE and EME are reported as cumulative event numbers, whereas the NE bursts are reported as *counts per second* (cps). For all the specimens, the observed bursts can be clearly correlated to the loading peak.

As regards the NE measurements, the He^3 neutron detector was switched on at least one hour before the beginning of each compression test, in order to reach the thermal equilibrium in electronics and to make sure that the behaviour of the device were stable with respect to intrinsic thermal effects. For the considered specimens, the average measured background level ranges from $(5.13 \pm 1.28) \times 10^{-2}$ to $(5.41 \pm 1.35) \times 10^{-2}$ cps. In general, neutron measurements for specimens G-50–0.5 and G-50–1.0 yielded values comparable to the natural background, whereas in specimens G-50–2.0 and in Quartz specimens the experimental data exceeded the background value by three/four times, approximately. In Table 2, the frequencies of AE and EME are reported together with the neutron flux at the peak load for three slendernesses of micro-crystalline Gypsum (three identical specimens per each slenderness), for two slendernesses of macro-crystalline Gypsum (three identical specimens per each slenderness), and for five irregular specimens of Quartz.

4. Nuclear and stoichiometric balances

In Table 3 and Fig. 5, EDS results for C, O, Si, and Mg concentrations on external surfaces and on fracture surfaces of micro-crystalline Gypsum specimens are shown. Considering the mean values of the two distributions over the fifteen investigated spots, the increments and decrements are reported. The stoichiometric balances, which are based on the assumed nuclear balances (fission-LENR), reproduce the experimental data very accurately. The only significant divergence regards the Carbon increment, which experimentally appears to be equal to 5.9 % against 5.5 % of the theoretical prediction.

In Table 4 and Fig. 6, EDS results for C, O, S, and Ca concentrations on external surfaces and on fracture surfaces of macro-crystalline Gypsum specimens are shown. Considering the mean values of the two distributions over the fifteen investigated spots, the increments and decrements are reported. The stoichiometric balances, which are based on the assumed nuclear balances (fusion- and fission-LENR), reproduce the experimental data very accurately. The only significant divergence regards the Oxygen increment, which experimentally appears to be equal to 8.3 % against 3.7 % of the theoretical prediction.

Finally, in Table 5 and Fig. 7, EDS results for C, O, Si, N, S, and Ca concentrations on external surfaces and on fracture surfaces of Quartz specimens are shown. Considering the mean values of the two distributions over the fifteen investigated spots, the increments and decrements are reported. The stoichiometric balances, which are based on the assumed nuclear balances (prevalently fission-LENR), reproduce the experimental data very accurately. The only significant divergence regards the Carbon increment, which experimentally appears to be equal to 6.5 % against 6.2 % of the theoretical prediction.

5. Conclusions

Extensive experimental investigations were conducted on Gypsum and Quartz compression specimens of different sizes. They were brought to complete failure, showing two different failure modalities: (1) Very brittle loading drop for micro-crystalline Gypsum and

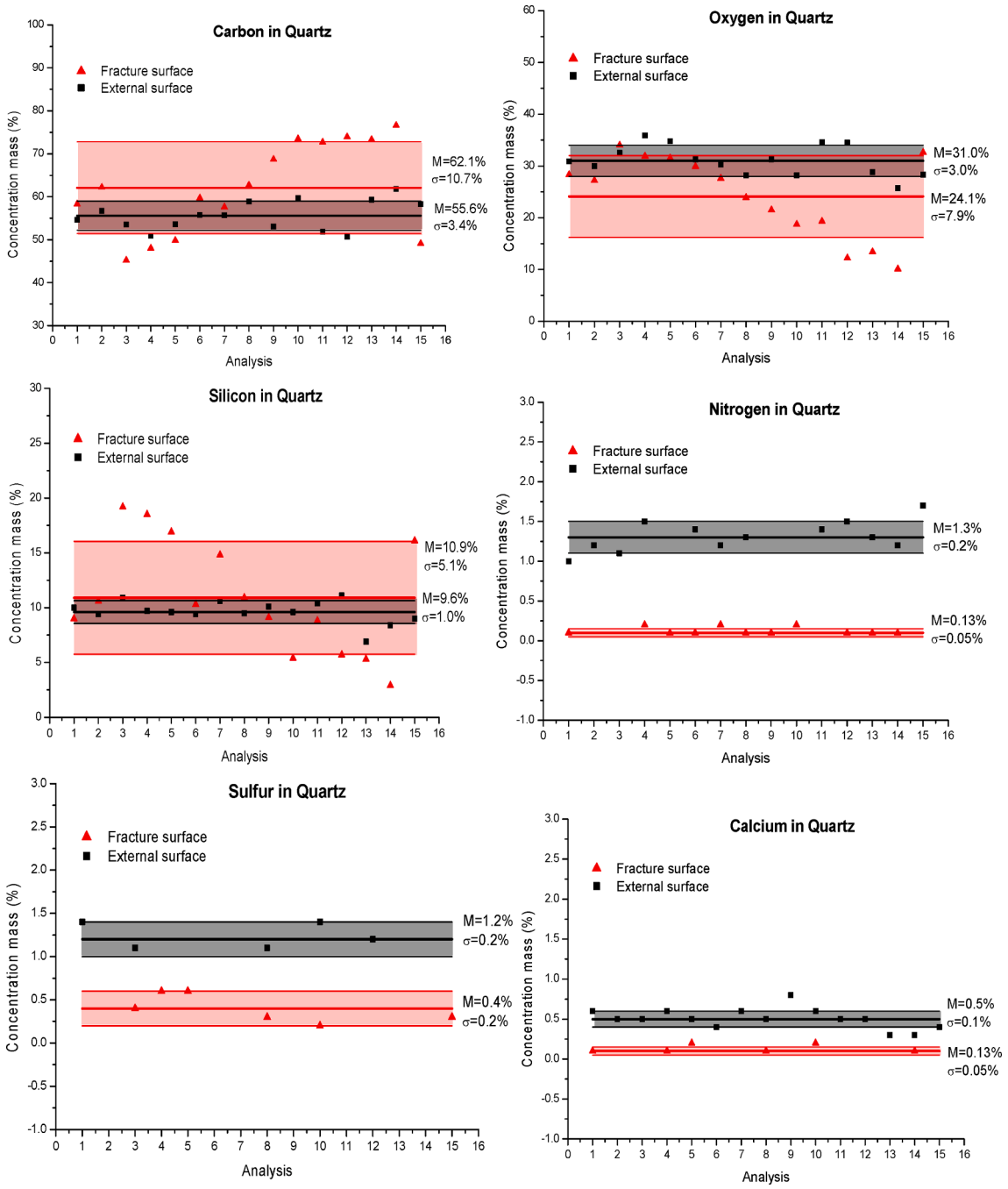

Fig. 7. EDS results for C, O, Si, N, S, and Ca concentrations in quartz: (a) C concentration on external surfaces (black squares) and on fracture surfaces (red triangles); (b) O concentration on external surfaces (black squares) and on fracture surfaces (red triangles); (c) Si concentration on external surfaces (black squares) and on fracture surfaces (red triangles); (d) N concentration on external surfaces (black squares) and on fracture surfaces (red triangles); (e) S concentration on external surfaces (black squares) and on fracture surfaces (red triangles); (f) Ca concentration on external surfaces (black squares) and on fracture surfaces (red triangles).

Quartz; (2) Stable strain-softening behaviour for macro-crystalline Gypsum. All the tested specimens emitted acoustic and electromagnetic waves and the single events cumulated up to the peak load. On the other hand, neutron emissions were evident only for the largest specimens, which are more brittle than the smaller ones. The significant chemical composition changes occurring on the fracture surfaces are consistently explained by the assumption of LENR, both fusion and fission reactions. It is the first time that fusion reactions emerge from crushing tests, whereas fission reactions have already explained the results related to other materials like the iron-rich natural rocks. Let us observe that, in the case of macro-crystalline Gypsum, an original correlation seems to appear between

mechanical behaviour (strain-softening) and LENR modalities (multi-body fusion reactions).

CRediT authorship contribution statement

Alberto CARPINTERI: Writing – original draft, Validation, Supervision, Project administration, Funding acquisition, Conceptualization. **Oscar BORLA:** Software, Investigation, Formal analysis, Data curation. **Federico ACCORNERO:** Writing – review & editing, Investigation.

Declaration of Competing Interest

The authors declare that they have no known competing financial interests or personal relationships that could have appeared to influence the work reported in this paper.

Data availability

Data will be made available on request.

Acknowledgements

This project has received funding from European Union's Horizon 2020 Research and Innovation Programme under Grant Agreement No. 951974. This work reflects only the authors' view and the Commission is not responsible for any use that may be made of the information it contains.

References

[1] Carpinteri A, Cardone F, Lacidogna G. Piezonuclear neutrons from brittle fracture: early results of mechanical compression tests. Strain 2009;45:332–9.
[2] Cardone F, Carpinteri A, Lacidogna G. Piezonuclear neutrons from fracturing of inert solids. Phys Lett A 2009;373:4158–63.
[3] Carpinteri A, Cardone F, Lacidogna G. Energy emissions from failure phenomena: mechanical, electromagnetic, nuclear. Exp Mech 2010;50:1235–43.
[4] Carpinteri A, Borla O, Lacidogna G, Manuello A. Neutron emissions in brittle rocks during compression tests: Monotonic vs cyclic loading. Phys Mesomech 2010; 13:268–74.
[5] Carpinteri A, Lacidogna G, Manuello A, Borla O. Energy emissions from brittle fracture: neutron measurements and geological evidences of piezonuclear reactions. Strength Fract Complexity 2011;7:13–31.
[6] Mogi K. Study of elastic shocks caused by the fracture of heterogeneous materials and its relation to earthquake phenomena. Bulletin of Earthquake Res Institute 1962;40:125–73.
[7] Lockner DA, Byerlee JD, Kuksenko V, Ponomarev A, Sidorin A. Quasi static fault growth and shear fracture energy in granite. Nature 1991;350:39–42.
[8] Ohtsu M. The history and development of acoustic emission in concrete engineering. Mag Concr Res 1996;48:321–30.
[9] Rundle JB, Turcotte DL, Shcherbakov R, Klein W, Sammis C. Statistical physics approach to understanding the multiscale dynamics of earthquake fault systems. Rev Geophys 2003;41:1019–49.
[10] Niccolini G, Schiavi A, Tarizzo P, Carpinteri A, Lacidogna G and Manuello A (2010). Scaling in temporal occurrence of quasi-rigid-body vibration pulses due to macrofractures. *Physical Review E* 82:46115/1-46115/5.
[11] Carpinteri A, Lacidogna G. Damage monitoring of an historical masonry building by the acoustic emission technique. Mater Struct 2006;39:161–7.
[12] Carpinteri A, Lacidogna G. Structural monitoring and integrity assessment of medieval towers. J Struct Engng *(ASCE)* 2006;132:1681–90.
[13] Carpinteri A, Lacidogna G. Damage evaluation of three masonry towers by acoustic emission. Engng Struct 2007;29:1569–79.
[14] Lacidogna G, Carpinteri A, Manuello A, Durin G, Schiavi A, Niccolini G, et al. Acoustic and electromagnetic emissions as precursor phenomena in failure processes. Strain 2010;47(2):144–52.
[15] Carpinteri A, Lacidogna G, Manuello A, Niccolini G, Schiavi A, Agosto A. Mechanical and electromagnetic emissions related to stress-induced cracks. Exp Tech 2010;36(3):53–64.
[16] Misra A. Theoretical study of the fracture-induced magnetic effect in ferromagnetic materials. Phys Lett A 1977;62:234–6.
[17] Frid V, Rabinovitch A, Bahat D. Fracture induced electromagnetic radiation. J Phys D 2003;36:1620–8.
[18] Hadjicontis V, Mavromatou C, Nonos D. Stress induced polarization currents and electromagnetic emission from rocks and ionic crystals, accompanying their deformation. Nat Haz Earth System Sci 2004;4:633–9.
[19] Warwick JW, Stoker C, Meyer TR. Radio emission associated with rock fracture: possible application to the great Chilean earthquake of May 22, 1960. J Geophys Res 1982;87:2851–9.
[20] Nagao T, Enomoto Y, Fujinawa Y, et al. Electromagnetic anomalies associated with 1995 Kobe earthquake. J Geodyn 2002;33:401–11.
[21] Rabinovitch A, Frid V, Bahat D. Surface oscillations. A possible source of fracture induced electromagnetic oscillations. Tectonophysics 2007;431:15–21.
[22] Widom A, Swain J, Srivastava YN. Neutron production from the fracture of piezoelectric rocks. J Phys G: Nucl Part Phys 2013;40:15006.
[23] Widom A, Swain J, Srivastava YN. Photo-disintegration of the iron nucleus in fractured magnetite rocks with magnetostriction. Meccanica 2015;50:1205–16.
[24] Lucia U, Carpinteri A. GeV plasmons and spalling neutrons from crushing of iron-rich natural rocks. Chem Phys Lett 2015;640:112–4.
[25] Carpinteri A, Lucia U, Zucchetti M and Borla O (2022). THz vibrations and phono-fission reactions from crushing of iron-rich natural rocks. *J Condensed Matter Nuclear Sci.* In press.
[26] Carpinteri A, Borla O. Nano-scale fracture phenomena and TeraHertz pressure waves as the fundamental reasons for geochemical evolution. Strength Fract Complexity 2018;11:149–68.
[27] Carpinteri A, Borla O. Fracto-emissions as seismic precursors. Engng Fract Mech 2017;177:239–50.
[28] Carpinteri A, Borla O. Acoustic, electromagnetic, and neutron emissions as seismic precursors: the lunar periodicity of low-magnitude seismic swarms. Engng Fract Mech 2019;210:29–41.
[29] Carpinteri A, Manuello A., Borla O. Hydrogen embrittlement, microcracking, and THz vibrations in the metal electrodes of cold-fusion electrolysis experiments: repeatability of nuclear and stoichiometric balances. *J Condensed Matter Nuclear Sci.* In press.